

RESEARCH PAPER



## New pyrazolopyrazoline derivatives as dual acting antimalarial-antileishmanial agents: synthesis, biological evaluation and molecular modelling simulations

Adnan A. Bekhit<sup>a,b,c</sup> , Eskedar T. Lodebo<sup>c,d</sup>, Ariaya Hymete<sup>c</sup>, Hanan M. Ragab<sup>a</sup>, Salma A. Bekhit<sup>e</sup>, Kikuko Amagase<sup>f</sup>, Afnan Batubara<sup>g</sup>, Mohammed A. S. Abourehab<sup>h,i</sup>, Alaa El-Din A. Bekhit<sup>j</sup>  and Tamer M. Ibrahim<sup>k</sup> 

<sup>a</sup>Department of Pharmaceutical Chemistry, Faculty of Pharmacy, Alexandria University, Alexandria, Egypt; <sup>b</sup>Pharmacy Program, Allied Health Department, College of Health and Sport Sciences, University of Bahrain, Zallaq, Kingdom of Bahrain; <sup>c</sup>Department of Pharmaceutical Chemistry and Pharmacognosy, School of Pharmacy, Addis Ababa University, Addis Ababa, Ethiopia; <sup>d</sup>Department of Chemistry, Kotebe Metropolitan University, Addis Ababa, Ethiopia; <sup>e</sup>High Institute of Public Health, Alexandria University, Alexandria, Egypt; <sup>f</sup>Laboratory of Pharmacology & Pharmacotherapeutics, College of Pharmaceutical Sciences, Ritsumeikan University, Kusatsu, Japan; <sup>g</sup>Department of Pharmaceutical Chemistry, College of Pharmacy, Umm Al-Qurra University, Makkah, Saudi Arabia; <sup>h</sup>Department of Pharmaceutics, College of Pharmacy, Umm Al-Qura University, Makkah, Saudi Arabia; <sup>i</sup>Department of Pharmaceutics and Industrial Pharmacy, Faculty of Pharmacy, Minia University, Minia, Egypt; <sup>j</sup>Food Sciences, University of Otago, Dunedin, New Zealand; <sup>k</sup>Department of Pharmaceutical Chemistry, Faculty of Pharmacy, Kafrelsheikh University, Kafr El-Sheikh, Egypt

### ABSTRACT

Promising inhibitory activities of the parasite multiplication were obtained upon evaluation of *in vivo* antimalarial activities of new pyrazolopyrazoline derivatives against *Plasmodium berghei* infected mice. Further evaluation of **5b** and **6a** against chloroquine-resistant strain (RKL9) of *P. falciparum* showed higher potency than chloroquine. *In vitro* antileishmanial activity testing against *Leishmania aethiopica* promastigote and amastigote forms indicated that **5b**, **6a** and **7b** possessed promising activity compared to miltefosine and amphotericin B deoxycholate. Moreover, antileishmanial activity reversal of the active compounds *via* folic and folinic acids showed comparable results to the positive control trimethoprim, indicating an antifolate mechanism *via* targeting leishmanial DHFR and PTR1. The compounds were non-toxic at 125, 250 and 500 mg/kg. In addition, docking of the most active compound against putative malarial target *Pf*-DHFR-TS and leishmanial PTR1 rationalised the observed activities. Molecular dynamics simulations confirmed a stable and high potential binding of **7a** against leishmanial PTR1.

### ARTICLE HISTORY

Received 8 June 2022  
Revised 9 August 2022  
Accepted 21 August 2022

### KEYWORDS

Pyrazoline derivatives;  
antimalarial evaluation;  
antileishmanial evaluation;  
antifolate mechanism;  
molecular docking;  
molecular dynamics

## 1. Introduction

Malaria and leishmaniasis have emerged as thoughtful health problems throughout the history of manhood. According to WHO Report in 2019, although there is a considerable deterioration in the number of malaria cases and deaths, the disease accounts for 228 million cases globally and is one of the top causes of death for children in Africa<sup>1</sup>. Despite the efforts in introducing a great number of chemotherapeutic agents to treat malaria, there is still an urgent medical need in the area. The main reason for this is the emergence of resistance<sup>2,3</sup>. Resistance has occurred for almost all therapeutic agents approved for the treatment of malaria which represents a major apprehension demanding an instant action<sup>1,3</sup>. Therefore, the search for newer and more effective drugs has become a crucial target.

Leishmaniasis is a complex disease that is caused by more than 20 species of *Leishmania* and is correlated to several clinical manifestations ranging from simple skin lesions around the bite site to fatal visceral forms<sup>4,5</sup>. More than one billion people are at risk of leishmaniasis in endemic areas<sup>6,7</sup>. Therefore, there is a continuing necessity to discover new antiprotozoal agents that are

effective against multidrug-resistant parasites and inhibitors that target enzymes and proteins macromolecules<sup>8,9</sup>. For the folate pathway, dihydrofolate Reductase (DHFR) and Pteridine reductase (PTR1) are validated targets for leishmania<sup>10</sup>. Their main role is to reduce oxidised pteridines like biopterin and folate to active cofactors tetrahydrobiopterin (THB) and tetrahydrofolate (THF), respectively. Nonetheless, utmost leishmania species showed resistance against DHFR-TS inhibitors<sup>11,12</sup>, owing to the presence of an alternative salvage pathway regulated by PTR1. Interestingly, the PTR1 enzyme is overexpressed in strains that exhibited antifolate resistance, hence, offering the means to bypass the dihydrofolate reductase-thymidylate synthase (DHFR-TS) pathway<sup>13–15</sup>.

It is well known that pyrazole rings, whether free or conjugated with other heterocyclic rings, demonstrated a wide collection of biological activities, such as antibacterial, antiviral, antitubercular, anti-inflammatory, antioxidant, anticancer, antimalarial and anti-leishmanial<sup>16–29</sup>. Also, derivatives containing pyrazoline scaffold were reported to show promising antileishmanial and/or antimalarial effects in a low micromolar range of activities (**I** and **II** in Figure 1)<sup>30,31</sup>. Interestingly, as we reported earlier, when integrating a pyrazole scaffold in a pyrazoline framework, yielded a

**CONTACT** Tamer M. Ibrahim  [Tamer.ibrahim2@gmail.com](mailto:Tamer.ibrahim2@gmail.com), [Tamer\\_Mohamad@pharm.kfs.edu.eg](mailto:Tamer_Mohamad@pharm.kfs.edu.eg)  Department of Pharmaceutical Chemistry, Faculty of Pharmacy, Kafrelsheikh University, Kafr El-Sheikh, 33516, Egypt; Adnan A. Bekhit  [adnbekhit@hotmail.com](mailto:adnbekhit@hotmail.com), [adnbekhit@pharmacy.alexu.edu.eg](mailto:adnbekhit@pharmacy.alexu.edu.eg)  Pharmacy Program, Allied Health Department, College of Health and Sport Sciences, University of Bahrain, Kingdom of Bahrain, P.O. Box 32038

 Supplemental data for this article can be accessed online at <https://doi.org/10.1080/14756366.2022.2117316>.

© 2022 The Author(s). Published by Informa UK Limited, trading as Taylor & Francis Group.

This is an Open Access article distributed under the terms of the Creative Commons Attribution-NonCommercial License (<http://creativecommons.org/licenses/by-nc/4.0/>), which permits unrestricted non-commercial use, distribution, and reproduction in any medium, provided the original work is properly cited.

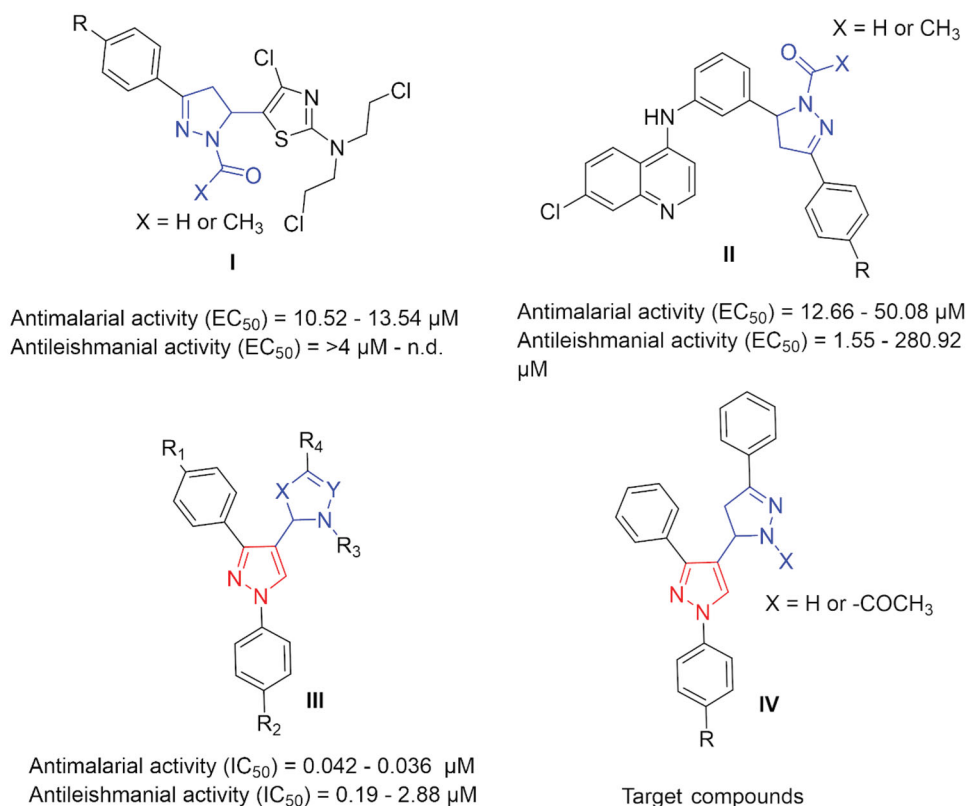


**Figure 1.** Some previously reported pyrazoline derivatives (I and II) and pyrazole hybrids with other heterocyclic moieties (III) with dual antimalarial and antileishmanial activity. Compounds (IV) represent our target compounds.

promising sub-micromolar range of activities for both antimalarial and antileishmanial effects (III in Figure 1)<sup>32</sup>. These interesting biological activity profiles inspired us to synthesise focussed derivatives of pyrazole integrated pyrazoline analogues as potential antimalarial and/or antileishmanial agents (IV).

The synthesised compounds were evaluated for their antimalarial activity using *Plasmodium berghei* infected mice (*in vivo* approach) where the most active compounds were further evaluated against chloroquine-resistant strain (RKL9) of *P. falciparum* (*in vitro* approach). For the antileishmanial activity, the compounds were screened against both promastigote and amastigote forms of *Leishmania aethiopica*. The reversal of the antileishmanial activity *via* folic and folinic acid confirmed the antifolate mechanism of the synthesised compounds anticipating PTR1 inhibition. Furthermore, docking experiments on putative malarial Pf-DHFR-TS and leishmanial PTR1 targets rationalised the observed antimalarial and antileishmanial activities.

## 2. Results and discussion

### 2.1. Chemistry

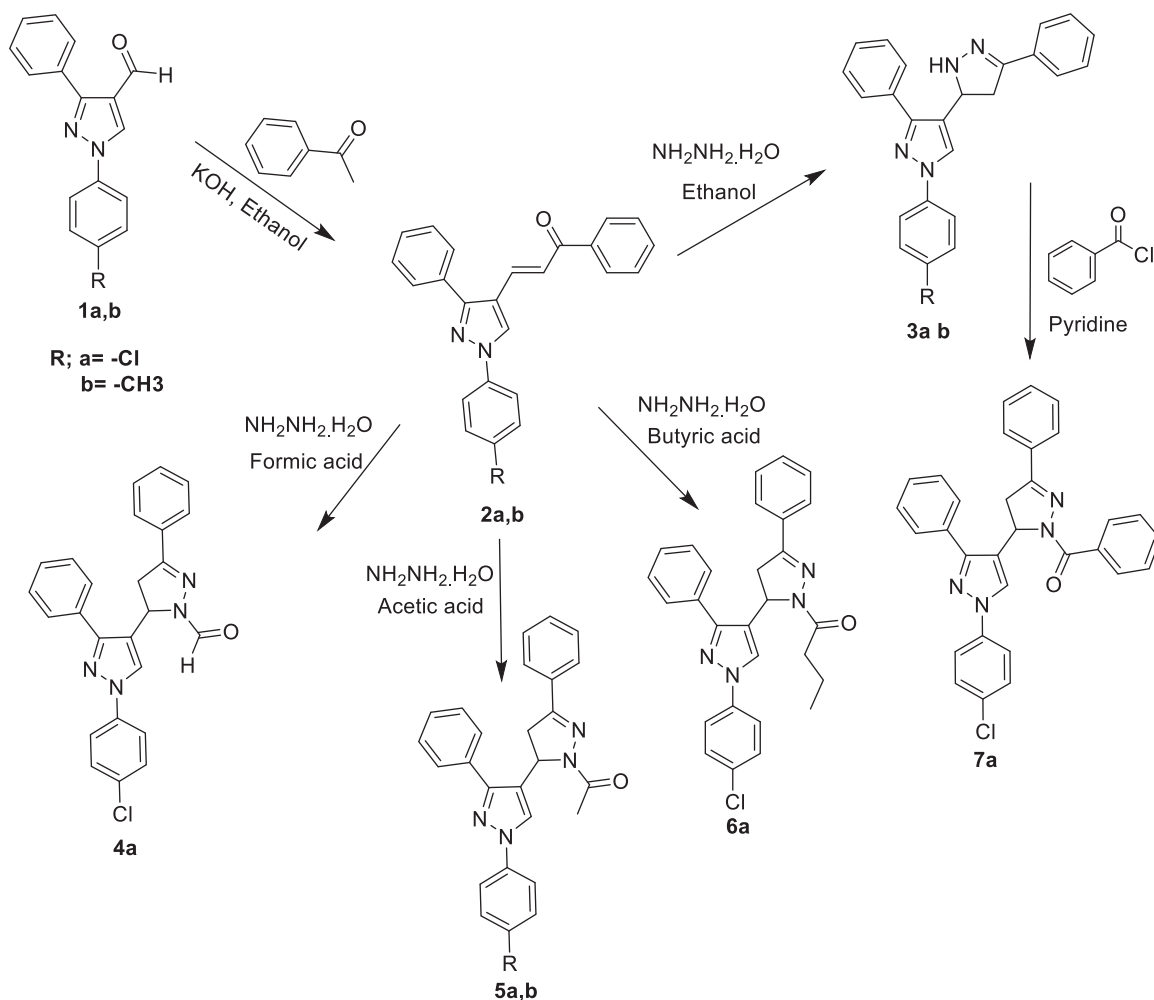
The target compounds were synthesised according to the steps outlined in Scheme 1. Initially, the two intermediate chalcones **2a,b** containing  $\alpha$ ,  $\beta$ -unsaturated ketone group were synthesised by condensation of aldehydes **1a,b**<sup>33</sup> and acetophenone in the presence of KOH in ethanol. The structures of these compounds were confirmed by IR spectra that showed the absence of characteristic peaks at 2726 and 2669  $\text{cm}^{-1}$  which was attributed to the C-H stretching vibration of the aldehydic groups of **1a,b**. Moreover, the <sup>1</sup>H-NMR spectrum of these two compounds revealed the disappearance of the singlet at  $\delta$  10.1 attributed to the aldehydic peak in addition to the presence of two doublets at

$\delta$  equals 7.4 and 7.9 corresponding to the methine protons which confirms the formation of the target compounds. The two formed chalcones were cyclized by refluxing with hydrazine hydrate in presence of different solvents like ethanol, formic acid, acetic acid and butyric acid to give the corresponding pyrazolylpyrazoline derivatives **3a**, **3b**, **4a**, **5a**, **5b** and **6a**. The structures of the formed derivatives were proved by the absence of a characteristic intense band around 1665  $\text{cm}^{-1}$  that corresponds to the C=O and the aldehydic characteristic peaks at 2726 and 2669  $\text{cm}^{-1}$  of their IR spectra. In addition, characteristic peaks for the formation of pyrazoline moiety have been observed on their <sup>1</sup>H-NMR spectra. These are methylene protons at the C<sub>4</sub> of the pyrazoline ring resonated as two doublets of doublet peaks (both integrated for one proton each) at 3.05–3.15 and 3.4–3.55 ppm. The C<sub>5</sub> proton peak appeared as a doublet of a doublet at 5.08–5.18 ppm due to vicinal coupling with the two magnetically non-equivalent protons of the methylene group at the C<sub>4</sub> position of the pyrazoline ring. The strong deshielding of the C<sub>5</sub> protons compared with the C<sub>4</sub> protons of the pyrazoline ring was assumed to be due to electron withdrawing neighbours. Finally, the benzoyl derivative of compound **7a** was synthesised by refluxing the unsubstituted pyrazolylpyrazoline **3a** with benzoyl chloride in presence of pyridine. Generally, the spectral aspects of the pyrazolyl derivatives were confirmed and guided by previous studies<sup>32,34</sup>. Representative NMR charts can be found in the Supplementary Material.

### 2.2. Biological activity

#### 2.2.1. *In vivo* antimalarial activity testing against Plasmodium berghei

The *in vivo* biological activities of some of the synthesised pyrazolylpyrazoline derivatives showed promising results against *P.*



**Scheme 1.** General synthetic route of the target compounds.

**Table 1.** Antiplasmodial activities of the synthesised compounds at 20 mg/kg.

Test substance	Dose (mg/kg)	% Parasitaemia*	% Suppression
3a	20	54.3 ± 1.4	-3.8
3b	20	53.1 ± 1.3	-1.9
5b	20	18.8 ± 2.6	66.7
6a	20	30.3 ± 2.8	42.3
7a	20	33.0 ± 1.9	36.5
Chloroquine P.	20	0.0	100
NC**	1 ml/100 g	52.2 ± 3.1	0.0

\*Values are M ± SD,  $P < 0.05$ , \*\* Negative control.

**Table 2.** Antiplasmodial activities of the synthesised compounds at 30 mg/kg.

Test substance	Dose (mg/kg)	% Parasitaemia*	% Suppression
5b	30	17.4 ± 1.2	71.2
6a	30	28.3 ± 2.8	52.4
7a	30	41.1 ± 3.1	30.3
NC**	1 ml/100 g	59.3 ± 3.1	0.0

\*Values are M ± SD,  $P < 0.05$ , \*\*Negative control.

*berghei* (Tables 1 and 2). The *in vivo* antimalarial activity of the synthesised compounds was evaluated at a dose level of 20 mg/kg (Table 1). Those compounds that revealed statistically significant suppression ( $p < 0.05$ ) were further evaluated at a dose level of 30 mg/kg. Antimalarial testing at the second dose was carried out for three compounds (5b, 6a and 7a) to examine assay variability (Table 2).

By the end of the 4-day suppressive test, compound 6a at a dose level of 20 and 30 mg/kg showed mean parasitaemia of 30.3

and 28.3%, respectively, compared to 52.2 and 59.3% for the negative control (Tables 1 and 2). This specifies a 42.3 and 52.4% suppression for 6a compared to the negative control groups. The mice treated with chloroquine (positive control) were completely free of the parasite on day 4. The growth in percentage suppression with growing the dose of the tested compound is revealing of the presence of a dose-response relationship. Like 6a, 7a displayed significant parasitaemia suppressive effect on day 4 compared to the negative control (Tables 1 and 2). At the dose levels of 20 and 30 mg/kg, the mean parasitaemia for 7a was found to be 33.0 and 41.1%, respectively equivalent to 36.5 and 30.3% suppression of the parasite. However, the decrease in the suppressive effect of increasing the administered dose of 7a implies that the 30 mg/kg dose might have compromised the immune system of the tested mice. Compound 5b showed the most potent suppressive effect among the tested compounds, as seen in Tables 1 and 2. At the dose levels of 20 and 30 mg/kg the mean parasitaemia was found to be 18.8 and 17.4%, respectively equivalent to 66.7 and 71.2% suppression. Suppressive activity of compound 5b follows a dose-response relationship.

Elucidating some structure-activity relationship (SAR), the methyl substituent on the phenyl group and acetyl substituent on the pyrazoline ring favours the antiplasmodial activity (5b). The presence of bulkier substituents (butanoyl and benzoyl) on the pyrazoline ring appeared to correlate with the activity of compounds 6a and 7a. On the other hand, the absence of substituent on the pyrazoline ring in compound 3b abolished the activity. The

**Table 3.** *In vitro* anti-plasmodial activity against chloroquine-resistant (RKL9) strain of *P. falciparum*.

Comp. No.	IC <sub>50</sub> , μM ± SD*
<b>5b</b>	0.0368 ± 0.006
<b>6a</b>	0.0946 ± 0.002
Chloroquine	0.1920 ± 0.003
Pyrimethamine	0.01246 ± 0.002

\*Results of two separate determinations.

presence of smaller substituent (acetyl and formyl) or absence of substituent can correlate to the loss of activity in the case of *p*-chlorophenyl derivatives **3a**, **4a** and **5a**. Generally, owing to the uniqueness of such compounds as dual-acting antimalarial-antileishmanial hits, we would pursue more studies on them in the near future with a wider array of substituents, in order to extract sharper insights into the structure-activity relationships.

### 2.2.2. *In vitro* antimalarial activity testing against chloroquine-resistant (RKL9) strain of *Plasmodium falciparum*

Compounds **5b** and **6a** that showed the highest *in vivo* percent suppression against *P. berghei* at a dose level of 30 mg/Kg, were further evaluated for their antiplasmodial activities against chloroquine-resistant (RKL9) *P. falciparum* strain. Results revealed that both compounds showed greater activity than chloroquine phosphate (IC<sub>50</sub> = 0.1920 μM) against the chloroquine resistant (RKL9) strain of *P. falciparum*. Compound **5b** was the most potent against RKL9 strains showing around 6-fold higher inhibitory activity than chloroquine (Table 3). Comparing **5b** to a standard folate inhibitor (pyrimethamine), both were in a similar nano-molar range of inhibitory activity with a slight superiority of pyrimethamine. Interestingly, these results are in coherence with our previous report<sup>32</sup> where the *in vitro* antimalarial effect of pyrazole-pyrazoline hybrids was in a similar nano-molar range of activity.

### 2.2.3. *In vitro* antileishmanial activity on leishmania aethiopic promastigote and amastigote forms

The assay was used to determine the viability of promastigotes and evaluate the antileishmanial activity of the synthesised compounds. The tested compounds **5b**, **6a** and **7a** showed higher antileishmanial activity than the reference standard miltefosine, whereas compound **5b** exhibited comparable activity to the reference standard Amphotericin B deoxycholate (Table 4). The result indicated that the presence of a relatively bulky substituent on one of the pyrazolo-N<sub>1</sub> rather than its C<sub>5</sub> led to a high inhibitory effect on the promastigotes, with IC<sub>50</sub> values ranging from 0.05 to 0.89 μM. Furthermore, the presence of an alkyl group rather than hydrogen on the carbonyl of the N<sub>1</sub>-side chain also improves the antileishmanial activity as indicated by the results observed for compounds **5b**, **6a** and **7a**.

Compounds **5b** and **7a** exhibited good activity against *L. aethiopic* amastigotes close to the activity determined for miltefosine reference (Table 4). Overall, these promising results agree with our previous report<sup>32</sup> where the *in vitro* antileishmanial activity of pyrazole-pyrazoline hybrids was also in a sub-micromolar range of activity.

### 2.2.4. Reversal of the antileishmanial activity via folic and folinic acid

Leishmania parasites were exposed to the tested compounds or trimethoprim (the positive control) at concentrations above their IC<sub>50</sub> after the addition of either folinic or folic acids. Exposure of

**Table 4.** Antileishmanial activity is expressed as antipromastigote and antiamastigote activities of the test compounds and reference standards.

Comp. No.	Antileishmanial activity (IC <sub>50</sub> *)			
	Antipromastigote		Antiamastigote	
	μg/ml	μM	μg/ml	μM
<b>3a</b>	3.06 ± 0.12	9.13 ± 0.30	1.10 ± 0.18	2.76 ± 0.45
<b>3b</b>	4.11 ± 0.22	10.86 ± 0.58	2.82 ± 0.36	7.45 ± 0.95
<b>4a</b>	3.84 ± 0.14	9.02 ± 0.33	2.64 ± 0.12	6.18 ± 0.28
<b>5a</b>	3.64 ± 0.18	8.28 ± 0.41	1.89 ± 0.04	4.29 ± 0.09
<b>5b</b>	0.03 ± 0.24	0.05 ± 0.57	0.42 ± 0.32	1.00 ± 0.76
<b>6a</b>	0.42 ± 0.28	0.89 ± 0.60	0.68 ± 0.14	1.45 ± 0.30
<b>7a</b>	0.04 ± 0.24	0.08 ± 0.48	0.44 ± 0.22	0.87 ± 0.44
Miltefosine	3.19 ± 14	7.83 ± 0.34	0.30 ± 0.04	0.74 ± 0.10
Amphotericin B deoxycholate	0.05 ± 0.002	0.04 ± 0.001	0.20 ± 0.02	0.15 ± 0.01

\*IC<sub>50</sub>: values indicate the effective concentration of a compound required to achieve 50% growth inhibition in μg/ml.

the parasite to folinic or folic acid declined the antileishmanial effect of both the tested compounds and trimethoprim. Also, exposure to folic acid together with trimethoprim led to a rise in the parasite survival time up to 100%. This can be clarified by the fact that folic acid (a natural substrate) competed for the active site of PTR1 and leishmanial DHFR enzyme while folinic acid contributed to DNA synthesis without any need to undergo metabolism. Also, folic acid was observed to display greater inhibition of the antileishmanial activity of the tested compounds than folinic acid.

Furthermore, the addition of excess folic acid to parasitic cells after exposure to the tested compounds was performed to investigate its ability to reverse antileishmanial inhibition. All tested compounds and trimethoprim presented reversibility of the antileishmanial inhibition. This designates that the observed antileishmanial activity of the synthesised compounds are mediated via an antifolate mechanism anticipating both leishmanial DHFR and PTR1. Further insights on mechanistic details are elaborated in the modelling section and molecular dynamics simulations for the most active compound **7a**.

### 2.2.5. *In vivo* acute toxicity test

An acute toxicity study was conducted to assess the acute lethal, physical and behavioural effects of the most active compounds (**5b** and **6a**) after oral administration to mice, as reported earlier<sup>35</sup>. Oral administration of the two highly active compounds in doses of 125, 250 and 500 mg/kg did not show any significant acute toxic effects on the experimental mice, as shown in Table 5. The data indicated that no death was observed during the first 24 h of the experimental period in any of the test groups. The results of the study showed that the median lethal dose (LD<sub>50</sub>) of synthesised compounds is higher than 500 mg/kg/day for mice through the oral route.

## 2.3. Molecular Modelling

### 2.3.1. Molecular Docking

To elucidate a putative molecular mechanism for the antimalarial activity, we carried out docking experiments of the most active compounds against the quadruple mutant (N511, C59R, S108N and I164L) *Pf* DHFR-TS structure. Challenging the most active compounds by such a highly mutant model would provide clues about the *in silico* binding compared to the reference *Pf* DHFR-TS binder (pyrimethamine), especially in a resistant variant of malaria.

The docking scores of the most active compounds obviously indicated significant *in silico* binding towards the mutant *Pf*

**Table 5.** Data from the acute toxicity studies.

Test substances	Dose (mg/Kg)	Wt. before test* (Day 0)	Wt. after test* (Day 1)
<b>5b</b>	125	33.8 ± 1.2	33.3 ± 2.6
	250	32.2 ± 2.5	32.4 ± 2.0
	500	32.8 ± 2.8	32.5 ± 1.4
<b>6a</b>	125	31.3 ± 2.5	31.5 ± 1.8
	250	32.1 ± 1.7	31.8 ± 1.7
	500	32.2 ± 2.1	32.6 ± 1.3
<b>NC</b>	1 ml/100g	32.1 ± 1.9	32.6 ± 2.1

\*Values are M ± SD.

**Table 6.** AutoDock Vina docking scores (kcal mol<sup>-1</sup>) of the most active compounds against *Pf* DHFR-TS (PDB: 1j3k) and PTR1 (PDB: 2bfm).

	Docking score		
	<i>Pf</i> -DHFR-TS <sup>a</sup>	<i>Pf</i> -DHFR-TS <sup>b</sup>	Leishmanial PTR1
<b>5b</b>	-11.2	-9.8	-9.3
<b>7a</b>	-10.9	-10.4	-10.4
<b>6a</b>	-8.5	-7.6	-8.5
Pyrimethamine <sup>c</sup>	-7.7	-8.5	-
Dihydropterine <sup>d</sup>	-	-	-8.4
Trimethoprim <sup>d</sup>	-	-	-7.4

<sup>a</sup>Quadruple mutant (N51I, C59R, S108N and I164L) *Pf* DHFR-TS structure. <sup>b</sup>Wild-type *Pf* DHFR-TS structure. <sup>c</sup>Pyrimethamine is a binder to *Pf* DHFR-TS. <sup>d</sup>Dihydropterine and Trimethoprim are binders to PTR1.

DHFR-TS structure, especially when compared to the reference *Pf* DHFR-TS binder (pyrimethamine) as shown in Table 6. Interestingly, their docking scores on the quadruple mutant *Pf* DHFR-TS (resistant form) are superior to their respective scores against the wild-type *Pf* DHFR-TS. Particularly, **5b** (the most active compound) shows the best score compared to all compounds and is the reference for the quadruple mutant structure. This confirms their inhibitory power against the resistant forms of malaria (see Table 3). This is emphasised by the fact that pyrimethamine (the reference) displayed a worse score against the quadruple mutant compared to the wild-type. Furthermore, **5b** and **7a** still demonstrate superior scores compared to pyrimethamine against wild-type structure. This specifies a particular binding of the most active compounds towards the mutant *Pf* DHFR-TS structure as a possible resistance mechanism to malaria.

The docking pose of **5b**, the most active compound against the chloroquine-resistant (RKL9) strain of *P. falciparum* (see Tables 1–3), exhibits favourable interactions with the binding site residues of quadruple mutant *Pf*-DHFR-TS. H-bonding interaction can be observed with the 1-acetyl moiety (carbonyl group as H-bond acceptor) with the cofactor NADPH. Furthermore, the core of the **5b** pose appeared to be deeply packed in a hydrophobic region, as shown in Figure 2. For instance, the 1-acetyl-3-phenyl pyrazoline moiety is packed between the co-factor NADPH and the side chains of Met55, Ile14, Leu46, Ser111 and Phe58. Also, 3-phenyl pyrazole is surrounded by the side chains of Phe116, Met55, Pro113 and Leu119 indicating favourable hydrophobic interactions. Overall, the such postulated binding mode would block the catalytic activity of *Pf*-DHFR. Based on our analysis of the docking poses of different stereoisomers, we observed some perturbations in their docking scores indicating the importance of stereo-selectivity for *Pf*-DHFR binding.

To rationalise the antileishmanial activity and the antifolate mechanism of most active compounds, our attention was devoted primarily to the co-crystal structure of PTR1 as a putative target since the co-crystal structure of the leishmanial DHFR-TS enzyme has not been resolved yet. The most active compounds **5b**, **7a** and **6a** showed a superior docking score compared to

trimethoprim (a DHFR and PTR1 inhibitor) and dihydropterine (a natural substrate for PTR1), as seen in Table 6. Interestingly, the most active compound **7a** against both promastigote and amastigote forms of leishmania displays the best docking score compared to all compounds as well as both reference compounds. This anticipates favourable binding towards PTR1 and hence confirming the antifolate mechanism confirmed by the *in vitro* experiment (Section Reversal of the antileishmanial activity via folic and folinic acid).

The docking pose of **7a** shows mainly hydrophobic interactions with binding site residues blocking the catalytic activity, as seen in Figure 3. For instance, the 3-phenyl pyrazoline moiety is packed between the co-factor NADPH and the residues Val230, Leu188 and Pro115. The 1-benzoyl pyrazoline moiety demonstrates vdW interaction with Phe113 and hydrophobic interaction with NADPH. Also, 3-phenyl pyrazole group is packed between the residues Val230, Met233 and Pro115 indicating favourable hydrophobic interactions. Overall, the such postulated binding mode would block the catalytic activity of PTR1 and hence inhibiting the leishmanial folate pathway. Again, the poses of different stereoisomers showed differences in the docking scores designating the importance of stereo-selectivity for PTR1 binding.

To further confirm the stable binding of **7a** pose against leishmanial PTR1 in a time-dependent manner and hence validate PTR1 as a potential target in the folate pathway, we performed molecular dynamics simulation for three systems for 50 ns. The details can be found in the coming Section.

We performed additional docking experiments for the less active compounds **3a** and **3b** in the binding site of *Pf*-DHFR and PTR1. We did not find significant score differences between both compounds and the most active ones. The docking scores of **3a** and **3b** were identical (-11.2 kcal/mol) against *Pf*-DHFR, which is a comparable score to the range found in the most active compounds (Table 6). Likewise, the docking scores of **3a** and **3b** were -8.9 and -8.5 with PTR1, respectively. Again, this indicates a similar docking range to the most active compounds (Table 6). The observed *in-vitro* anti-leishmanial activity for these compounds (most and least active) lie within the low- and sub-micromolar range of activities. This would be highly challenging to yield significant differences in the output docking scores. Nevertheless, we assume that the lower activity of **3a** and **3b** can be attributable to their relatively lower lipophilicity compared to the most active compounds **6a** and **7a**. The calculated lipophilicity (via logP function of Marvin Sketch v17.2.6.0 – ChemAxon – <http://www.chemaxon.com>) for **3a**, **3b**, **5b**, **6a** and **7a** were 5.92, 5.83, 5.53, 6.77 and 7.48, respectively. Adequate lipophilicity would enable the ligand to diffuse sufficiently through the lipophilic membranes of the protozoa and reach the macromolecular target for binding events.

### 2.3.2. Molecular Dynamics simulation

The **7a** docking pose in PTR1 was subjected to 50 ns molecular dynamics (MD) simulations for evaluating the stability of its docked pose in a time-dependent manner in the binding site. Furthermore, another run was conducted for the apo PTR1 form and the complexed form with the co-crystal PTR1 structure, to account for its dynamicity as a reference. This results in a total of three MD runs, 50 ns each. Root Mean Square Deviation (RMSD) is a measure of protein backbone stability during the simulation time. RMSD of the apo and complexed with co-crystal ligand forms (Figure 4A) reach a converged state at 35 ns with a minor fluctuation in the 0.2 nm range. This reflects the appropriate

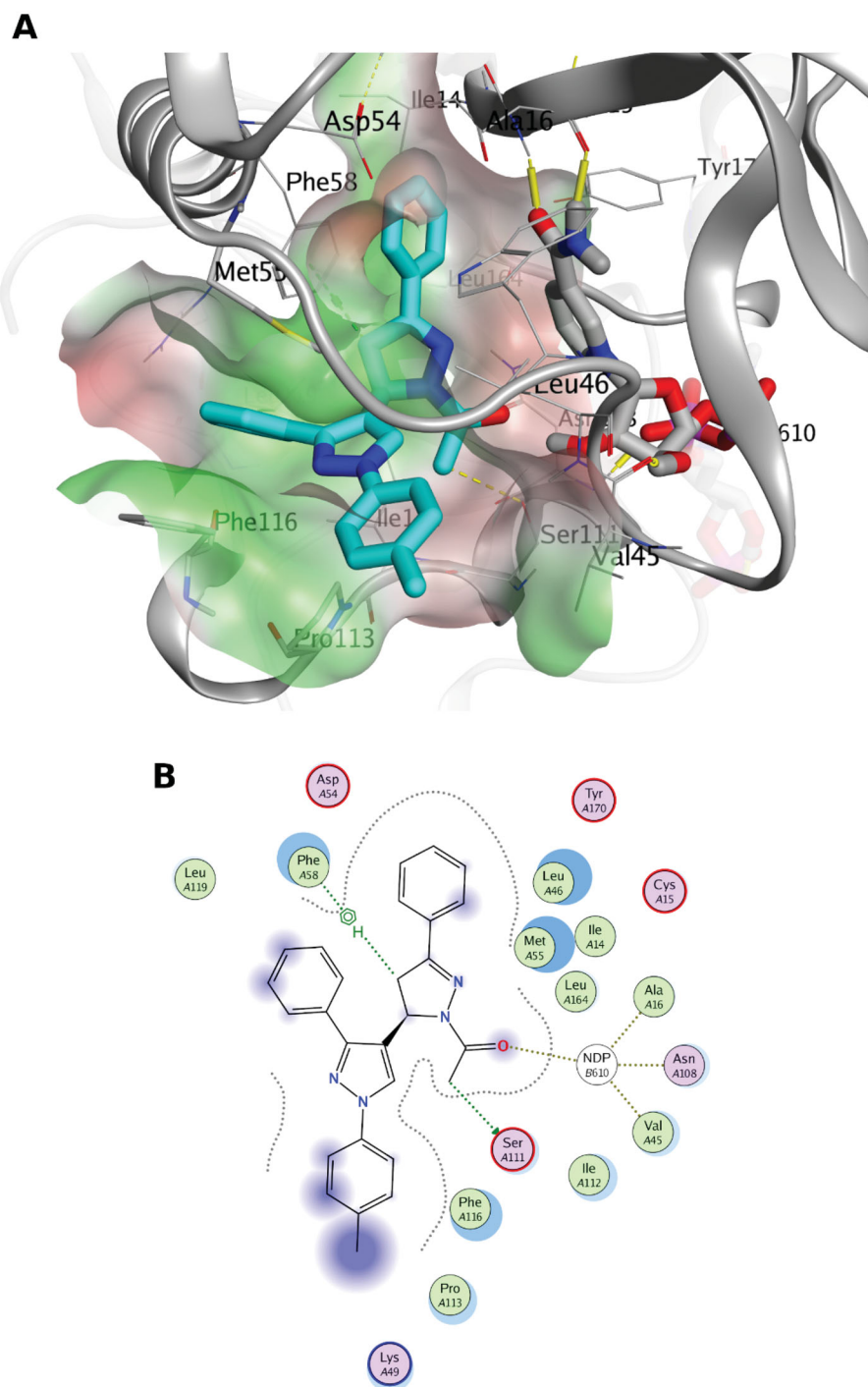


**Figure 2.** The docking pose of the most active compound (**5b**) as cyan sticks in the binding site of the quadruple mutant *Pf*-DHFR-TS (PDB code: 1j3k). The hydrophilic and hydrophobic regions are in red and green coloured molecular surfaces, respectively. Non-polar hydrogen atoms were omitted for clarity. The label “NDP-610” represents the NADPH co-factor.

stability of the protein structure during the two simulation runs. Interestingly, the RMSD profile of the complexed form with **7a** exhibited an earlier convergence at 25 ns and a steady state performance until the end of the simulation course. Minor variations of the protein backbone for both complexed forms (co-crystal ligand and **7a**) can be observed around 0.2 nm (2 Å) after convergence. This is also in coherence with analysis obtained by the Radius of gyration (Rg) in Figure 4(B). Rg is a measure of protein structure compactness during simulation time. There is no great fluctuation in the Rg of the protein complexed with **7a** compared to both the apo and co-crystal ligand complex structures since

they display an Rg range of 0.05 nm after 25000 frames (25 ns). This gives an indication of the low conformational changes of the protein throughout the simulation, and hence, its stability<sup>36,37</sup>. Per residue root means square fluctuation (RMSF) assesses the conformational changes that occur to each residue of the protein, as shown in Figure 4(C). The *N*-terminal amino acids exhibit the highest RMSF contemplated by the high free movement of their free loops. However, the key binding site amino acids (numbers: Asp232, Val230, Leu188, His241, Tyr191, Leu229, Met233, Phe113) show low RMSF (< 2.5 Å) and comparable fluctuation behaviour to all the three simulated protein forms. This highlights good

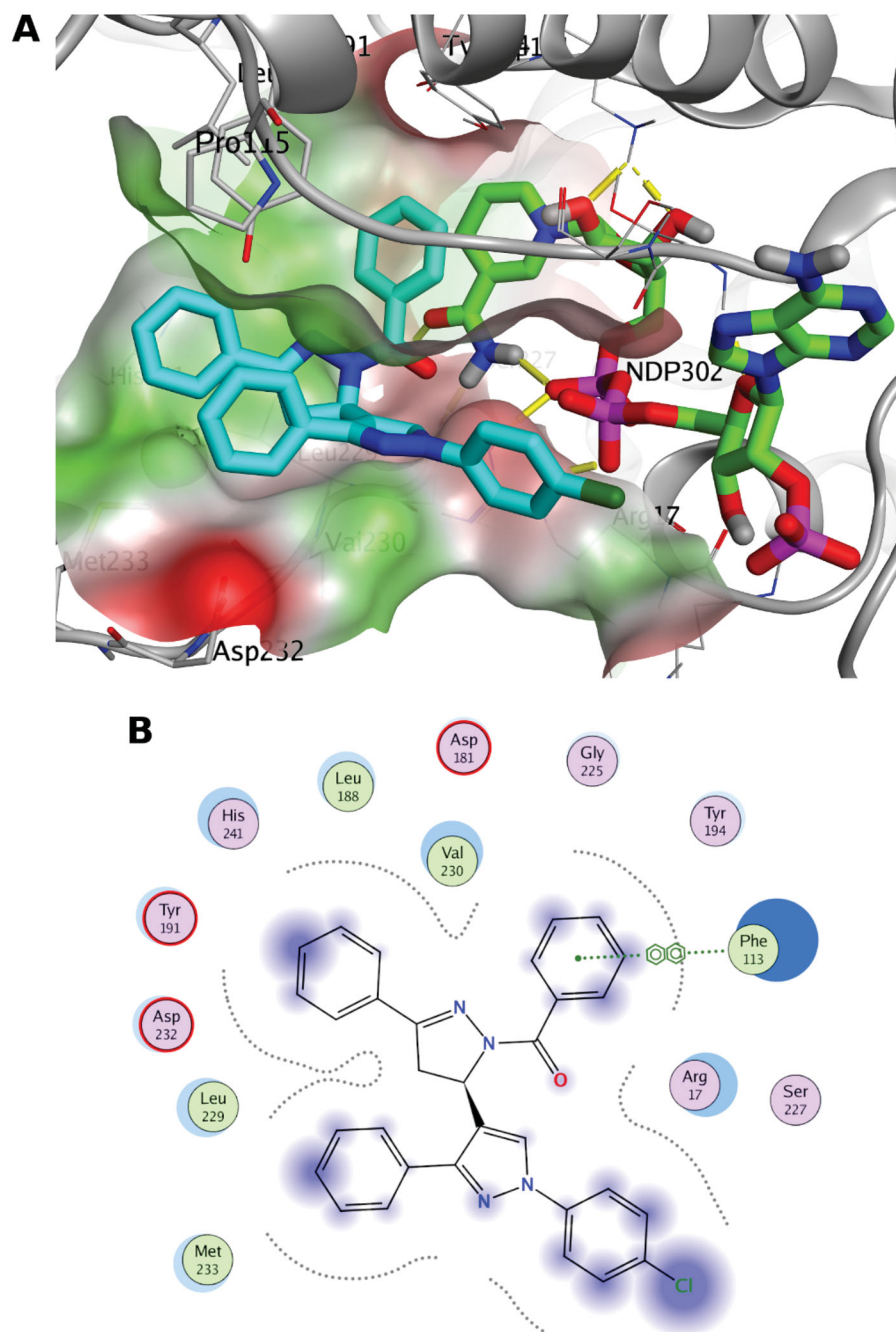


**Figure 3.** The docking pose of the most active compound (**7a**) as cyan sticks in the binding site of PTR1 (PDB code: 7pxx). The hydrophilic and hydrophobic regions are in red and green coloured molecular surfaces, respectively. Non-polar hydrogen atoms were omitted for clarity. The label “NDP-302” represents the NADPH co-factor.

binding of the complexed ligand (**7a**) and minimal conformational changes in these residues compared to the apo and co-crystal ligand complex forms. Such good binding is augmented by the analysis of the hydrogen bond count of **7a** pose in the binding site during the simulation time, as seen in Figure 4(D). It is obvious that at least one H-bonding interaction is formed all over the majority of 50 ns simulations.

To reveal the ligand positional deviation throughout the simulation, RMSD analysis of the non-hydrogen ligand atoms was performed across the simulation time (Figure 4E). From the beginning of the simulation until 20 ns time, both **7a** and co-crystal ligands deviated from their starting pose with some fluctuations around 0.5 nm and 0.75 nm RMSD. Interestingly, after 20 ns

both **7a** and the co-crystal ligand showed a comparable steady state with superior stability and lower divergence of the **7a** pose compared to the co-crystal ligand. This agrees with **7a** H-bond count behaviour since a persistent H-bond was formed after 20 ns contributing to it is stable binding in the binding site of PTR1.

We utilised the principal component analysis (PCA) to analyse the conformational sampling of the PTR-1 systems in the simulated subspace via examining their dominant modes of motion. The covariance matrix of atomic fluctuations was diagonalised for predicting the eigenvalues. The first few eigenvectors play a crucial role in the motions of the protein. The first 3 eigenvectors have a larger eigenvalue for the apo structure compared to both **7a** and co-crystal complexed forms of PTR1 systems. This reflects

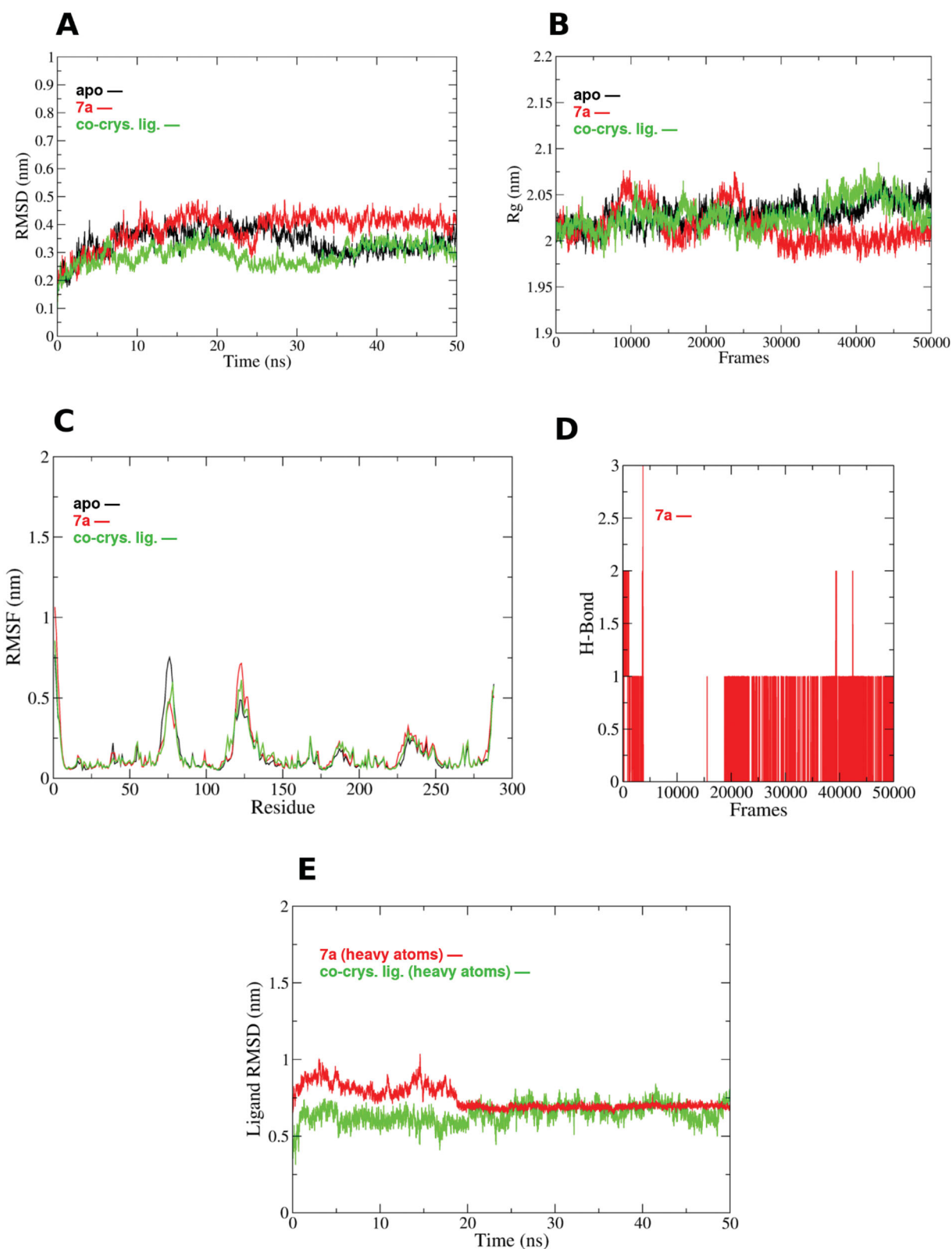


**Figure 4.** MD simulations for the three systems, the apo leishmanial PTR1, 7a-PTR1 complex and co-crystal ligand – PTR1 complex systems. (A) Root mean square deviation (RMSD) of the protein alpha carbon atoms across the 50 ns simulation. (B) The radius of gyration (Rg) for the PTR1 protein across the 50 ns simulation time. The frame number (x-axis) 5000 indicates 50 ns simulation time. (C) Per residue, root means square fluctuation (RMSF). (D) Hydrogen bond counts during the MD simulation for 7a in the binding site during the 50 ns simulation. (E) RMSD of the ligand heavy atoms during the 50 ns simulation of the ligand-complexed systems.

greater collective atomic fluctuations of the apo form and implies that the systems complexed with 7a or co-crystal ligand demonstrated reduced motions compared to the apo form.

To reveal the ligand influences on the conformational heterogeneity of PTR1, associated free energy landscapes (FEL) were determined as a function of the top two principal components

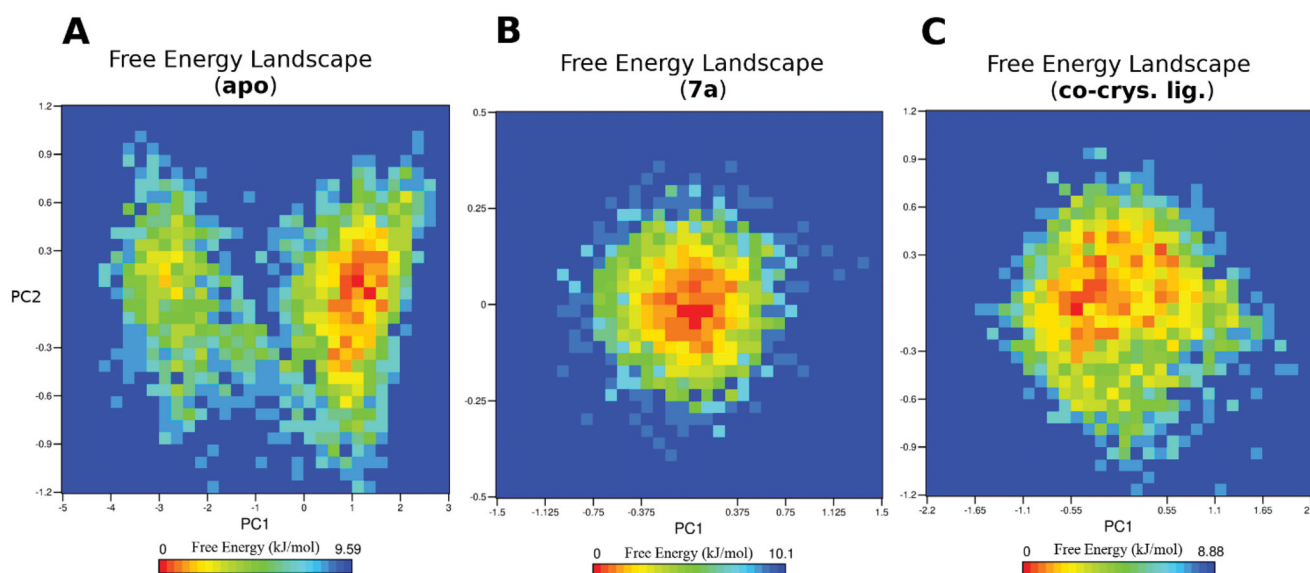


**Figure 5.** The free energy landscape (FEL) of the simulated PTR1 systems is based on the principal component analysis. (A) Leishmanial PTR1. (B) **7a**-PTR1 complex. (C) Co-crystal ligand – PTR1 complex. The colour bar represents the free energy value in kcal mol<sup>-1</sup>. The colour ranges from red to yellow to blue spots indicate the energy minima and energetically favoured protein conformations to more unfavourable high-energy conformations.

(PC1 and PC2), as illustrated in Figure 5. FEL can be used to effectively describe conformational redistributions provoked by binding events<sup>38,39</sup>. Figure 5 shows the relative conformational changes of the protein backbone of the three simulated systems. The deeper colour (towards the red colour) in the plot reveals lower-energy conformational metastable states. Interestingly, the simulated apo system of PTR1 visits two separate energy basins, one represents the global minimum of the simulated subspace, while the other is quite narrow and separated by conformations with a low energy barrier from the main basin. This reflects the presence of diverse ensembles of flexible and low-energy conformations during 50 ns simulation. On the other hand, both ligand-complexed systems display comparable FEL profiles implying one main energy basin of the simulated subspace. For instance, the **7a** complexed structure is populated by a single and a focussed energy basin indicating a concise range of metastable states during the 50 ns simulation. Likewise, the co-crystal ligand complexed system exhibits similar pattern to the **7a** system, however, with a wider energy basin. These results thus clearly highlight that **7a** binding to PTR1 can alter the PTR1 conformational subspace towards low energy conformations, and therefore, modulate its function. Overall, the results of the MD simulations confirmed the high potential and stable binding of **7a** to PTR1 augmenting the *in vitro* antileishmanial through the antifolate mechanism.

### 3 Material and methods

#### 3.1. Chemistry

Melting points were determined in open glass capillaries using electro thermal BUCHI (B-540) hot storage melting-point apparatus and are uncorrected. Infra-red (IR) spectra were recorded on Shimadzu 8400SP infra-red spectrophotometer using nujol. <sup>1</sup>H-NMR spectra were recorded on Bruker Avance DMX400 400 MHz FT-NMR spectrometer using DMSO-d<sub>6</sub> as a solvent and the chemical shifts are given in  $\delta$  (ppm) downfield from tetramethylsilane (TMS) which served as an internal standard. Splitting patterns were designated as follows: s: singlet; d: doublet; m: multiplet. Elemental analyses were performed on Perkin Elmer 2400 elemental analyser and were found within  $\pm 0.4\%$  of the theoretical

values. Follow-up of the reactions and checking of the purity of the compounds was made by thin layer chromatography (TLC) on silica gel-precoated aluminium sheets (Type 60 GF254, Merck) and the spots were detected by exposure to an iodine chamber for a few minutes.

#### 3.1.1 1-Aryl-3-phenyl-4-(3-phenyl-3-oxopropenyl)-1H-pyrazole (**2a,b**)

A mixture of the appropriate aldehyde **1a,b** (15 mmol)<sup>33</sup> and an equimolar amount of acetophenone (1.86 ml) was dissolved in 15 ml of ethanol, and 10 ml of 3% alcoholic KOH was added. The reaction mixture was stirred using a magnetic stirrer at room temperature for 6 h. The resulting solution was then allowed to stand overnight. The formed yellow precipitate was filtered, washed with ethanol, dried and recrystallised from ethanol.

#### 3.1.2 1-(4-Chlorophenyl)-3-phenyl-4-(3-phenyl-3-oxopropenyl)-1H-pyrazole (**2a**)

Yield, 72.4%; mp, 191–193 °C; IR (Nujol) cm<sup>-1</sup>: 1665 (C=O); 1610 (C=N); 1456 (C-Cl). <sup>1</sup>H-NMR (DMSO-d<sub>6</sub>)  $\delta$ (ppm): 7.4 (d, 1H,  $J$  = 15.6 Hz, methine-H), 7.4–7.7 (m, 10H, phenyl-H), 7.82 (d, 2H,  $J$  = 7.6 Hz *p*-chlorophenyl-C<sub>3,5</sub>H), 7.9 (d, 1H,  $J$  = 16.0 Hz, methine-H), 8.0 (d, 2H,  $J$  = 7.1 Hz *p*-chlorophenyl-C<sub>2,6</sub>H), 8.4 (s, 1H, pyrazole-C<sub>5</sub>H). Analysis calculated for C<sub>24</sub>H<sub>17</sub>ClN<sub>2</sub>O (384.86): C, 74.90; H, 4.45; N, 7.28; Cl, 9.21. Found: C, 75.21; H, 4.71; N, 7.53; Cl, 9.05. R<sub>f</sub> [benzene/ethyl acetate (9:1)] = 0.74.

#### 3.1.3 1-(4-Methylphenyl)-3-phenyl-4-(3-phenyl-3-oxopropenyl)-1H-pyrazole (**2b**)

Yield, 77.7%; mp, 176–178 °C; IR (Nujol) cm<sup>-1</sup>: 1660 (C=O); 1595 (C=N). <sup>1</sup>H-NMR (DMSO-d<sub>6</sub>)  $\delta$ (ppm): 7.4 (d, 1H,  $J$  = 15.6 Hz, methine-H), 7.38–7.65 (m, 10H, phenyl-H), 7.82 (d, 2H,  $J$  = 7.6 Hz, *p*-chlorophenyl-C<sub>3,5</sub>H), 7.9 (d, 1H,  $J$  = 15.9 Hz, methine-H), 7.98 (d, 2H,  $J$  = 7.1 Hz, *p*-chlorophenyl-C<sub>2,6</sub>H), 8.4 (s, 1H, pyrazole-C<sub>5</sub>H). Analysis calculated for C<sub>25</sub>H<sub>20</sub>N<sub>2</sub>O (364.44): C, 82.39; H, 5.53; N, 7.70. Found: C, 82.70; H, 5.24; N, 7.91. R<sub>f</sub> [benzene/ethyl acetate (9:1)] = 0.80.

**3.1.4 1-Aryl-3-phenyl-4-(3-phenyl-2-pyrazolin-5-yl)-1H-pyrazole (3a,b)**

A mixture of **2a,b** (2.6 mmol) and an equimolar amount of hydrazine hydrate (0.13 ml) was dissolved in 15 ml of ethanol. The mixture was heated under reflux for 30 min with continuous stirring using a magnetic stirrer. The reaction mixture was then cooled and the formed white precipitate was filtered, washed with ethanol, dried and recrystallised from ethanol.

**3.1.5 1-(4-Chlorophenyl)-3-phenyl-4-(3-phenyl-2-pyrazolin-5-yl)-1H-pyrazole (3a)**

Yield, 78.6%; mp, 207–209 °C; IR (Nujol)  $\text{cm}^{-1}$ : 3314 (N-H); 1600 (C=N); 1455 (C-Cl).  $^1\text{H-NMR}$  (DMSO- $d_6$ )  $\delta$ (ppm): 3.05–3.15 (dd, 1H,  $J=4.6$ , 17.6 Hz, pyrazoline- $\text{C}_4\text{H}$ ), 3.4–3.55 (dd, 1H,  $J=11.6$ , 17.6 Hz, pyrazoline- $\text{C}_4\text{H}$ ), 5.08–5.18 (dd, 1H,  $J=4.6$ , 11.6 Hz, pyrazoline- $\text{C}_5\text{H}$ ), 7.25–7.75 (m, 15H, *p*-chlorophenyl-H, phenyl-H, pyrazoline-NH), 8.05 (s, 1H, pyrazole- $\text{C}_5\text{H}$ ). Analysis calculated for  $\text{C}_{24}\text{H}_{19}\text{ClN}_4$  (398.89): C, 72.27; H, 4.80; N, 14.05; Cl, 8.89. Found: C, 72.56; H, 5.01; N, 13.91; Cl, 8.70.  $R_f$  [benzene/ethyl acetate (9:1)] = 0.57.

**3.1.6 1-(4-Methylphenyl)-3-phenyl-4-(3-phenyl-2-pyrazolin-5-yl)-1H-pyrazole (3b)**

Yield, 75.76%; mp, 211–213 °C; IR ( $\text{cm}^{-1}$ ): 3322 (N-H); 1600 (C=N).  $^1\text{H-NMR}$  (DMSO- $d_6$ )  $\delta$ (ppm): 2.3 (s, 3H,  $\text{CH}_3$ ), 3.1–3.2 (dd, 1H,  $J=4.5$ , 17.5 Hz, pyrazoline- $\text{C}_4\text{H}$ ), 3.6–3.7 (dd, 1H,  $J=11.5$ , 17.5 Hz, pyrazoline- $\text{C}_4\text{H}$ ), 5.8–5.9 (dd, 1H,  $J=4.5$ , 11.6 Hz, pyrazoline- $\text{C}_5\text{H}$ ), 7.18–7.68 (m, 15H, *p*-methylphenyl-H, phenyl-H, pyrazoline-NH), 7.8 (s, 1H, pyrazole- $\text{C}_5\text{H}$ ). Analysis calculated for  $\text{C}_{25}\text{H}_{22}\text{N}_4$  (378.47): C, 79.34; H, 5.86; N, 14.80. Found: C, 79.62; H, 6.08; N, 15.15.  $R_f$  [benzene/ethyl acetate (9:1)] = 0.61

**3.1.7 1-(4-Chlorophenyl)-3-phenyl-4-(1-formyl-3-phenyl-2-pyrazolin-5-yl)-1H-pyrazole (4a)**

A mixture of **2a** (1.3 mmol, 0.50 gm) and equimolar amount of hydrazine hydrate (0.07 ml) was dissolved in 20 ml of formic acid. The mixture was heated under reflux for 6 h with continuous stirring using a magnetic stirrer. The reaction mixture was then cooled and the formed white precipitate was filtered, washed, dried and recrystallised from ethanol. Yield, 72.7%; mp, 221–223 °C; IR (Nujol)  $\text{cm}^{-1}$ : 1667 (C=O); 1600 (C=N); 1446 (C-Cl).  $^1\text{H-NMR}$  (DMSO- $d_6$ )  $\delta$ (ppm): 3.1–3.2 (dd, 1H,  $J=4.6$ , 17.6 Hz, pyrazoline- $\text{C}_4\text{H}$ ), 3.7–3.8 (dd, 1H,  $J=11.6$ , 17.6 Hz, pyrazoline- $\text{C}_4\text{H}$ ), 5.7–5.8 (dd, 1H,  $J=4.6$ , 11.6 Hz, pyrazoline- $\text{C}_5\text{H}$ ), 7.25–7.7 (m, 14H, *p*-chlorophenyl-H, phenyl-H), 7.9 (s, 1H, pyrazole- $\text{C}_5\text{H}$ ), 8.9 (s, 1H, CHO). Analysis calculated for  $\text{C}_{25}\text{H}_{19}\text{ClN}_4\text{O}$  (426.90): C, 70.34; H, 4.49; N, 13.12; Cl, 8.30. Found: C, 70.51; H, 4.31; N, 12.87; Cl, 8.51.  $R_f$  [benzene/ethyl acetate (9:1)] = 0.55.

**3.1.8 1-(4-Chlorophenyl)-3-phenyl-4-(1-acetyl-3-phenyl-2-pyrazolin-5-yl)-1H-pyrazole (5a,b)**

A mixture of **2a,b** (1.3 mmol) and an equimolar amount of hydrazine hydrate (0.07 ml) was dissolved in 15 ml of glacial acetic acid. The mixture was heated under reflux for 4 h with continuous stirring using a magnetic stirrer. The reaction mixture was then cooled and the formed white precipitate was filtered, washed, dried and recrystallised from ethanol.

**3.1.9 1-(4-Chlorophenyl)-3-phenyl-4-(1-acetyl-3-phenyl-2-pyrazolin-5-yl)-1H-pyrazole (5a)**

Yield, 75.4%; mp, 233–236 °C; IR (Nujol)  $\text{cm}^{-1}$ : 1665 (C=O); 1595 (C=N); 1455 (C-Cl).  $^1\text{H-NMR}$  (DMSO- $d_6$ )  $\delta$ (ppm): 2.5 (s, 3H,  $\text{CH}_3$ ), 3.1–3.2 (dd, 1H,  $J=4.4$ , 17.4 Hz, pyrazoline- $\text{C}_4\text{H}$ ), 3.6–3.7 (dd, 1H,  $J=11.8$ , 17.4 Hz, pyrazoline- $\text{C}_4\text{H}$ ), 5.8–5.9 (dd, 1H,  $J=4.3$ , 11.7 Hz, pyrazoline- $\text{C}_5\text{H}$ ), 7.25–7.78 (m, 14H, *p*-chlorophenyl-H, phenyl-H), 7.81 (s, 1H, pyrazole- $\text{C}_5\text{H}$ ). Analysis calculated for  $\text{C}_{26}\text{H}_{21}\text{ClN}_4\text{O}$  (440.92): C, 70.82; H, 4.80; N, 12.71; Cl, 8.04. Found: C, 70.68; H, 4.72; N, 12.38; Cl, 8.19.  $R_f$  [benzene/ethyl acetate (9:1)] = 0.59.

**3.1.10 1-(4-Methylphenyl)-3-phenyl-4-(1-acetyl-3-phenyl-2-pyrazolin-5-yl)-1H-pyrazole (5b)**

Yield, 70.40%; mp, 217–219 °C; IR (Nujol)  $\text{cm}^{-1}$ : 1670 (C=O); 1615 (C=N).  $^1\text{H-NMR}$  (DMSO- $d_6$ )  $\delta$ (ppm): 2.3 (s, 3H, *p*-methylphenyl-H), 2.4 (s, 3H, acetyl-H), 3.1–3.2 (dd, 1H,  $J=4.4$ , 17.5 Hz, pyrazoline- $\text{C}_4\text{H}$ ), 3.6–3.7 (dd, 1H,  $J=11.6$ , 17.5 Hz, pyrazoline- $\text{C}_4\text{H}$ ), 5.8–5.9 (dd, 1H,  $J=4.4$ , 11.6 Hz, pyrazoline- $\text{C}_5\text{H}$ ), 7.18–7.68 (m, 14H, *p*-chlorophenyl-H, phenyl-H), 7.8 (s, 1H, pyrazole- $\text{C}_5\text{H}$ ). Analysis calculated for  $\text{C}_{27}\text{H}_{24}\text{N}_4\text{O}$  (420.51): C, 77.12; H, 5.75; N, 13.32. Found: C, 76.86; H, 5.47; N, 13.55.  $R_f$  [benzene/ethyl acetate (9:1)] = 0.65.

**3.1.11 1-(4-Chlorophenyl)-3-phenyl-4-(1-butanoyl-3-phenyl-2-pyrazolin-5-yl)-1H-pyrazole (6a)**

A mixture of **2a** (1.3 mmol, 0.5 gm) and an equimolar amount of hydrazine hydrate (0.07 ml) was dissolved in 15 ml of butyric acid. The mixture was heated under reflux for 6 h with continuous stirring using a magnetic stirrer. The reaction mixture was then concentrated, cooled and poured onto crushed ice (30 g). Finally, the white precipitate formed was filtered, washed with water, dried and recrystallised from ethanol: water (6:1) mixture. Yield, 78.65%; mp, 235–237 °C; IR (Nujol)  $\text{cm}^{-1}$ : 1665 (C=O); 1600 (C=N); 1450 (C-Cl).  $^1\text{H-NMR}$  (DMSO- $d_6$ )  $\delta$ (ppm): 1.0–1.1 (t, 3H,  $\text{CH}_3$ ), 1.7–1.9 (m, 2H,  $\text{CH}_2\text{CH}_3$ ), 2.7–2.9 (m, 2H,  $\text{CH}_2\text{CH}_2$ ), 3.1–3.2 (dd, 1H,  $J=4.5$ , 17.4 Hz, pyrazoline- $\text{C}_4\text{H}$ ), 3.6–3.7 (dd, 1H,  $J=11.7$ , 17.4 Hz, pyrazoline- $\text{C}_4\text{H}$ ), 5.8–5.9 (dd, 1H,  $J=4.5$ , 11.6 Hz, pyrazoline- $\text{C}_5\text{H}$ ), 7.25–7.78 (m, 14H, *p*-chlorophenyl-H, phenyl-H), 7.8 (s, 1H, pyrazole- $\text{C}_5\text{H}$ ). Analysis calculated for  $\text{C}_{28}\text{H}_{25}\text{ClN}_4\text{O}$  (468.98): C, 71.71; H, 5.37; N, 11.95; Cl, 7.56. Found: C, 71.94; H, 5.61; N, 11.84; Cl, 7.38.  $R_f$  [benzene/ethyl acetate (9:1)] = 0.62.

**3.1.12 1-(4-Chlorophenyl)-3-phenyl-4-(1-benzoyl-3-phenyl-2-pyrazolin-5-yl)-1H-pyrazole (7a)**

To a solution of **3a** (1.2 mmol, 0.48 gm) in dry pyridine (5 ml) an equivalent amount of benzoyl chloride (0.20 ml) was added. The reaction mixture was then heated in a boiling water bath for 20 min, cooled and poured onto crushed ice (30 g). The white precipitate formed was separated by filtration, washed with water, dried and recrystallised from ethanol. Yield, 75.4%; mp, 237–239 °C; IR ( $\text{cm}^{-1}$ ): 1650 (C=O); 1605 (C=N); 1455 (C-Cl).  $^1\text{H-NMR}$  (DMSO- $d_6$ )  $\delta$ (ppm): 3.2–3.3 (dd, 1H,  $J=4.8$ , 17.4 Hz, pyrazoline- $\text{C}_4\text{H}$ ), 3.8–3.9 (dd, 1H,  $J=11.8$ , 17.8 Hz, pyrazoline- $\text{C}_5\text{H}$ ), 6.0–6.1 (dd, 1H,  $J=4.6$ , 12.0 Hz, pyrazoline- $\text{C}_5\text{H}$ ), 7.25–7.95 (m, 19H, *p*-chlorophenyl-H, phenyl-H), 8.2 (s, 1H, pyrazole- $\text{C}_5\text{H}$ ). Analysis calculated for  $\text{C}_{31}\text{H}_{23}\text{ClN}_4\text{O}$  (502.99): C, 74.02; H, 4.61; N, 11.14; Cl, 7.05. Found: C, 73.79; H, 4.83; N, 10.88; Cl, 7.21.  $R_f$  [benzene/ethyl acetate (9:1)] = 0.70.

## 3.2. Biological evaluation

### 3.2.1. *In vivo* antimalarial activity testing against *Plasmodium berghei*

The *in vivo* antimalarial activities of the synthesised compounds were performed by using the standard 4-day suppressive test as described by Fidock et al.<sup>40</sup>. The practical procedures were performed as described earlier<sup>32</sup>. Briefly, Swiss albino mice of both sexes, weighing 24–38 g and 4–6 weeks of age, were acclimatised for a period of 7 days at room temperature (23–25 °C) and relative humidity of 60–65%. On day 0, the test mice were injected intravenously with 0.2 ml of  $2 \times 10^7$  parasitised erythrocytes infected with *P. berghei* ANKA strain. After 2 h of injection, the infected mice were weighed and arbitrarily divided into 37 groups of five mice per cage. Groups 1–35 (35 cages) received the compounds orally, each at 20 mg/kg dose levels and served as treatment groups. Group 36 received the drug vehicle (7% Tween, 3% ethanol in distilled water) and served as a negative control, while Group 37 received chloroquine phosphate at the dose level of 20 mg/kg and served as a positive control. On days 1–3, the treatment groups were treated with the same single dose of the synthesised compound at 24 h intervals. On day 4 (i.e. 24 h after the last dose), a blood smear from all test animals was prepared using Giemsa stain. The level of parasitemia was determined microscopically by counting 5 fields of approximately 100 erythrocytes per field. The difference between the mean value for the negative control group (taken as 100%) and those of the experimental groups was calculated and expressed as percent suppression or activity. Chloroquine-treated mice were completely cured of the parasite. The *in vivo* antimalarial activity testing procedure was repeated for three compounds (**5b**, **6a** and **7a**) at a dose level of 30 mg/Kg since they showed better percent suppression than the other compounds.

### 3.2.2. *In vitro* antimalarial activity testing against chloroquine-resistant (RKL9) strain of *Plasmodium falciparum*

The *P. falciparum* strain RKL9 was maintained in continuous culture using the standard method described by Trager and Jensen<sup>41</sup>. Compounds (**5b** and **6a**), the two most active compounds at a dose level of 30 mg/Kg, were further examined for their antiplasmodial activities against chloroquine resistant (RKL9) *P. falciparum* strain as reported earlier<sup>32</sup>.

### 3.2.3. *In vitro* antileishmanial activity on *L. aethiopia promastigotes* and *amastigote* forms

All the tested compounds were evaluated for their antileishmanial activity on both the promastigote and amastigote forms as reported earlier<sup>32</sup>.

### 3.2.4. Reversal of the antileishmanial activity via folic and folinic acid

This test was carried out on the *in vitro* growth assay for promastigotes and based on the previously published methodology<sup>42</sup>. All experimental steps were performed as reported earlier<sup>43</sup>.

### 3.2.5. *In vivo* acute toxicity test

Compounds that have shown good activity (**5b** and **6a**) were tested for their oral acute toxicity in mice according to previously reported procedures<sup>35</sup>. Four groups of animals each group consisting of six male mice were used for testing acute toxicity. Mice in

groups one and two were given 125 and 250 mg/kg/day of the synthesised compounds respectively and the third group was given the highest dose (500 mg/kg/day) and the fourth group was treated with the vehicle (control group) at a maximum dose volume of 1 ml/100 g of body weight by oral route. After the substance has been administered, food was withheld for a further 2 h period. The mice were observed closely as reported earlier<sup>44,45</sup>.

## 3.3. Molecular Modelling

### 3.3.1. Molecular docking

The prepared structure of the quadruple mutant (N51I, C59R, S108N and I164L) *Pf* DHFR-TS (PDB code:1j3k) was adapted from previous reports<sup>26,27</sup>. The leishmanial PTR1 (PDB: 7pxx) was retrieved from the Protein Data Bank (PDB) and prepared using "Quickprep" and "Structure Preparation" modules of MOE. The PDB files were converted to PDBQT files by employing a python script (*prepare\_receptor4.py*) provided by the MGLTools package (version 1.5.4)<sup>46</sup> for AutoDock Vina (version 1.1.2)<sup>47</sup> docking experiments.

The most active compounds (**5b**, **6a** and **7a**) and their stereoisomers were built and prepared by MOE as reported earlier<sup>26</sup>. The resulting conformers were saved as an SD files for the docking experiments. The SD files were converted and split into PDB files by MOE, which was further converted into PDBQT files by an MGLTools (version 1.5.4) python script (*prepare\_ligand4.py*) for AutoDock Vina docking experiments.

AutoDock Vina (version 1.1.2) was used for docking experiments of the most active compounds against both quadruple mutants (N51I, C59R, S108N and I164L) *Pf* DHFR-TS and leishmanial PTR1 structures. We employed default docking parameters and the size of the docking grid was  $22 \text{ \AA} \times 22 \text{ \AA} \times 22 \text{ \AA}$ , with a grid spacing of 1 Å. The centre of the grid box was adjusted on the centre of mass of the co-crystallized ligands. By default, the docking was terminated when the maximum energy difference between the best-scored pose and the worst one was 3 kcal/mol. This docking setup was validated by a successful pose-retrieval docking experiment for the co-crystal ligand on both PDB crystal structures.

### 3.3.2. Molecular Dynamics

The molecular dynamics simulations were carried out as reported earlier in some procedures<sup>48,49</sup>. Molecular dynamics simulations and systems build-up were carried out using GROMACS 2020.3<sup>50</sup>. The protein-ligand complex was solvated in a triclinic box of SPC216 with explicit water model<sup>51</sup>. The system was then neutralised by NaCl molecules at 0.1 M concentration. A steepest descent minimisation algorithm was applied for system energy minimisation setting 10 kJ/mol and 50,000 steps as convergence criteria. NVT followed by NPT equilibration was completed for 500 ps each at 300 K temperature and 1 atm pressure. Then, a production run was carried out for 50 ns at the NPT ensemble. The coordinates of the trajectory were saved each 10 ps time interval resulting in 5000 frames for the whole 50 ns simulation time. The V-rescale modified Berendsen thermostat<sup>52</sup> was used for temperature coupling for each equilibration run, while Berendsen coupling<sup>53</sup> was used for pressure coupling with a 2 ps time constant for equilibration and production runs. However, Parrinello-Rahman pressure coupling scheme<sup>54</sup> was employed for pressure coupling for the production runs. A Verlet cut-off scheme was used for searching neighbouring atoms and Van Der Waals calculations with cut-off and switch list distances of 1.2 and 1.0 nm, respectively. Particle

Mesh Ewald method<sup>55</sup> was used for the calculations of long-range electrostatics within 1.2 nm. Bond lengths were constrained using the LINear Constraint Solver (LINCS) algorithm<sup>56</sup>. CHARMM36 all-atom force field<sup>57</sup> was used for topology and parameter generation of the protein molecules, and SwissParam server<sup>58</sup> was used for ligand parameterisation. For all simulations, a leap-frog integrator was used with a steps size of 2 fs. Different analysis metrics, such as root mean squared deviation (RMSD), the radius of gyration (Rg), root mean squared fluctuation (RMSF), hydrogen-bond (H-bond) count, PCA (principal component analysis), and free energy landscape (FEL) were calculated via GROMACS and MDtraj tools<sup>59</sup> and some were plotted using XMGRACE<sup>60</sup>.

## 4 Conclusion

Nine target pyrazoline compounds were synthesised in acceptable yields (70–78%). The *in vivo* antimalarial activity of the synthesised compounds was evaluated against *P. berghei*. Compounds **5b**, **6a** and **7a** showed inhibition of the parasite multiplication by 66.7, 42.3 and 36.5%, respectively, at a dose level of 20 mg/kg; and 71.2, 52.4 and 30.3%, respectively, at a dose level of 30 mg/kg. The two most active compounds (**5b** and **6a**) were evaluated *in vitro* for their antimalarial activity against chloroquine-resistant strain (RKL9) of *P. falciparum* and were both found to be more potent than the standard chloroquine with IC<sub>50</sub> values of 0.0368 and 0.0946 μM, respectively.

The compounds were evaluated for their *in vitro* antileishmanial activity against *Leishmania aethiopica* promastigote and amastigote forms. Interestingly, the results showed that compounds **5b**, **6a** and **7b** were more potent than the standard miltefosine with IC<sub>50</sub> values of 0.05, 0.89 and 0.08 μM for the promastigote form, respectively. Furthermore, the reversal of antileishmanial activity of the active compounds *via* folic and folinic acids showed analogous results to the positive control Trimethoprim. This designates the antifolate mechanism for the antileishmanial activity of these compounds anticipating both leishmanial DHFR-TS and PTR1 enzymes as putative targets.

The *in vivo* acute toxicity test exhibited that **5b** and **6a** compounds were non-toxic at 125, 250 and 500 mg/kg. Molecular docking of the most active compounds against putative malarial Pf-DHFR-TS and leishmanial PTR1 targets justified the observed activities. The docking poses of **5b** and **7a** displayed superior performances compared to pyrimethamine against both wild-type and quadruple mutant (resistant) Pf-DHFR-TS, with superior scores towards the mutant form, implying high potential binding to the resistant Pf-DHFR-TS. Moreover, the most active compounds demonstrated a superior scores against the leishmanial PTR1 compared to the references, dihydropterine and trimethoprim. Interestingly, molecular dynamics simulations of three leishmanial PTR1 systems for 50 ns each, for the apo, the complexed with the most active **7a**, and the co-crystal complex systems, highlighted the stable and privileged binding of **7a** towards PTR1 in a time-dependent manner. These findings highlight that **7a** exerts its antileishmanial activity via inhibiting leishmanial PTR1.

## Acknowledgement

TMI would like to acknowledge Bibliotheca Alexandrina High-Performance Computing (BA-HPC) for granting access to perform the molecular dynamics simulations. The authors would like to thank the Deanship of Scientific Research at Umm Al-Qura University for supporting this work by Grant Code: (22UQU4290565DSR64).

## Author contributions

All authors have given approval to the final version of the manuscript. All authors agree to be accountable for the content of the work.

## Ethics statements

The animal study was reviewed and approved by the protocols used in this study followed the guidelines set in 'The Guide for the Care and Use of Laboratory Animals', and obtained approval by Animal Care & Use Committee (ACUC), Faculty of Pharmacy, Alexandria University, No. ACUC17/18 at 29/4/2017.

## Disclosure statement

The authors have no other relevant affiliations or financial involvement with any organisation or entity with a financial interest in or financial conflict with the subject matter or materials discussed in the manuscript apart from those disclosed.

## ORCID

Adnan A. Bekhit  <http://orcid.org/0000-0003-3865-0677>

Alaa El-Din A. Bekhit  <http://orcid.org/0000-0003-2569-8620>

Tamer M. Ibrahim  <http://orcid.org/0000-0003-1016-8950>

## References

1. W.H.O. World malaria report. <https://www.who.int/publications/i/item/9789241565721>; 2019.
2. Cheviet T, Wein S, Bourchenin G, et al. beta-hydroxy- and beta-aminophosphonate acyclonucleosides as potent inhibitors of *Plasmodium falciparum* growth. *J Med Chem* 2020;63: 8069–87.
3. Madhav H, Hoda N. An insight into the recent development of the clinical candidates for the treatment of malaria and their target proteins. *Eur J Med Chem* 2021;210:112955.
4. Goncalves GA, Spillere AR, das Neves GM, et al. Natural and synthetic coumarins as antileishmanial agents: a review. *Eur J Med Chem* 2020;203:112514.
5. Bekhit AA, El-Agroudy E, Helmy A, et al. Leishmania treatment and prevention: natural and synthesized drugs. *Eur J Med Chem* 2018;160:229–44.
6. Pigott DM, Bhatt S, Golding N, et al. Global distribution maps of the leishmaniasis. *eLife* 2014;3:e02851 1–21.
7. W.H.O., Leishmaniasis. [https://www.who.int/health-topics/leishmaniasis#tab=tab\\_1](https://www.who.int/health-topics/leishmaniasis#tab=tab_1); 2020.
8. Ogutu B. Artemether and lumefantrine for the treatment of uncomplicated *Plasmodium falciparum* malaria in sub-Saharan Africa. *Expert Opin Pharmacother* 2013;14:643–54.
9. Nwaka S, Hudson A. Innovative lead discovery strategies for tropical diseases. *Nat Rev Drug Discov* 2006;5:941–55.
10. Rajasekaran R, Chen YP. Potential therapeutic targets and the role of technology in developing novel antileishmanial drugs. *Drug Discov Today* 2015;20:958–68.
11. Vickers TJ, Beverley SM. Folate metabolic pathways in Leishmania. *Essays Biochem* 2011;51:63–80.
12. Nare B, Hardy LW, Beverley SM. The roles of pteridine reductase 1 and dihydrofolate reductase-thymidylate synthase in pteridine metabolism in the protozoan parasite Leishmania major. *J Biol Chem* 1997;272:13883–91.

13. Corona P, Gibellini F, Cavalli A, et al. Structure-based selectivity optimization of piperidine-pteridine derivatives as potent Leishmania pteridine reductase inhibitors. *J Med Chem* **2012**;55:8318–29.
14. Dube D, Periwal V, Kumar M, et al. 3D-QSAR based pharmacophore modeling and virtual screening for identification of novel pteridine reductase inhibitors. *J Mol Model* **2012**;18:1701–11.
15. de Souza Moreira D, Ferreira RF, Murta SMF. Molecular characterization and functional analysis of pteridine reductase in wild-type and antimony-resistant Leishmania lines. *Experiment Parasitol* **2016**;160:60–6.
16. Nayak N, Ramprasad J, Dalimba U. New INH-pyrazole analogs: design, synthesis and evaluation of antitubercular and antibacterial activity. *Bioorg Med Chem Lett* **2015**;25:5540–5.
17. Li Y-R, Li C, Liu J-C, et al. Synthesis and biological evaluation of 1,3-diaryl pyrazole derivatives as potential antibacterial and anti-inflammatory agents. *Bioorg Med Chem Lett* **2015**;25:5052–7.
18. Meng FJ, Sun T, Dong WZ, et al. Discovery of novel pyrazole derivatives as potent neuraminidase inhibitors against influenza H1N1 virus. *Archiv Der Pharmazie* **2016**;349:168–74.
19. Chuang H, Huang L-CS, Kapoor M, et al. Design and synthesis of pyridine-pyrazole-sulfonate derivatives as potential anti-HBV agents. *MedChemComm* **2016**;7:832–6.
20. Hafez HN, El-Gazzar A-RBA, Al-Hussain SA. Novel pyrazole derivatives with oxa/thiadiazolyl, pyrazolyl moieties and pyrazolo[4,3-d]-pyrimidine derivatives as potential antimicrobial and anticancer agents. *Bioorg Med Chem Lett* **2016**;26:2428–33.
21. Shi JB, Tang WJ, qi XB, et al. Novel pyrazole-5-carboxamide and pyrazole-pyrimidine derivatives: synthesis and anticancer activity. *Eur J Med Chem* **2015**;90:889–96.
22. Özdemir A, Altıntop MD, Kaplancıklı ZA, et al. Synthesis and evaluation of new 1, 5-Diaryl-3-[4-(methyl-sulfonyl) phenyl]-4, 5-dihydro-1H-pyrazole derivatives as potential antidepressant agents. *Molecules* **2015**;20:2668–84.
23. Viveka S, Dinesha D, Shama P, et al. Design, synthesis, anticonvulsant and analgesic studies of new pyrazole analogues: a Knoevenagel reaction approach. *RSC Advances* **2015**;5:94786–95.
24. Mabkhot YN, Kaal NA, Alterary S, et al. Synthesis, in-vitro antibacterial, antifungal, and molecular modeling of potent anti-microbial agents with a combined pyrazole and thiophene pharmacophore. *Molecules* **2015**;20:8712–29.
25. Faidallah HM, Al-Mohammadi MM, Alamry KA, Khan KA. Synthesis and biological evaluation of fluoropyrazolesulfonyleurea and thiourea derivatives as possible antidiabetic agents. *J Enzyme Inhib Med Chem* **2016**;31(Suppl 1):157–163.
26. Bekhit AA, Saudi MN, Hassan AMM, et al. Synthesis, in silico experiments and biological evaluation of 1,3,4-trisubstituted pyrazole derivatives as antimalarial agents. *Eur J Med Chem* **2019**;163:353–66.
27. Bekhit AA, Saudi MN, Hassan AM, et al. Synthesis, molecular modeling and biological screening of some pyrazole derivatives as antileishmanial agents. *Future Med Chem* **2018**;10:2325–44.
28. Tageldin GN, Fahmy SM, Ashour HM, et al. Design, synthesis and evaluation of some pyrazolo[3,4-d]pyrimidines as anti-inflammatory agents. *Bioorg Chem* **2018**;78:358–71.
29. Atta KFM, Ibrahim TM, Farahat OOM, et al. Synthesis, modeling and biological evaluation of hybrids from pyrazolo[1,5c]-pyrimidine as antileishmanial agents. *Future Med Chem* **2017**;9:1913–29.
30. Ramirez-Prada J, Robledo SM, Velez ID, et al. Synthesis of novel quinoline-based 4,5-dihydro-1H-pyrazoles as potential anticancer, antifungal, antibacterial and antiprotozoal agents. *Eur J Med Chem* **2017**;131:237–54.
31. Insuasty B, Ramirez J, Becerra D, et al. An efficient synthesis of new caffeine-based chalcones, pyrazolines and pyrazolo[3,4-b][1,4]diazepines as potential antimalarial, antitrypanosomal and antileishmanial agents. *Eur J Med Chem* **2015**;93:401–13.
32. Bekhit AA, Hassan AM, El Razik HAA, et al. New heterocyclic hybrids of pyrazole and its bioisosteres: design, synthesis and biological evaluation as dual acting antimalarial-antileishmanial agents. *Eur J Med Chem* **2015**;94:30–44.
33. Bekhit AA, Ashour HMA, Bekhit AE-DA, et al. Synthesis of some pyrazolyl benzenesulfonamide derivatives as dual anti-inflammatory antimicrobial agents. *J Enzyme Inhib Med Chem* **2009**;24:296–309.
34. Faour WH, Mroueh M, Daher CF, et al. Synthesis of some new amide-linked bipyrazoles and their evaluation as anti-inflammatory and analgesic agents. *J Enzyme Inhib Med Chem* **2016**;31:1079–94.
35. Bekhit AA, Baraka AM. Novel milrinone analogs of pyridine-3-carbonitrile derivatives as promising cardiotoxic agents. *Eur J Med Chem* **2005**;40:1405–13.
36. Arba M, Wahyudi ST, Brunt DJ, et al. Mechanistic insight on the remdesivir binding to RNA-Dependent RNA polymerase (RdRp) of SARS-cov-2. *Comp Biol Med* **2021**;129:104156.
37. Ismail MI, Ragab HM, Bekhit AA, Ibrahim TM. Targeting multiple conformations of SARS-CoV2 papain-like protease for drug repositioning: an in-silico study. *Comp Biol Med* **2021**;131:104295.
38. Pandey P, Rane JS, Chatterjee A, et al. Targeting SARS-CoV-2 spike protein of COVID-19 with naturally occurring phytochemicals: an in silico study for drug development. *J Biomol Struct Dyn* **2021**;39:6306–16.
39. Pandey P, Prasad K, Prakash A, Kumar V. Insights into the biased activity of dextromethorphan and haloperidol towards SARS-CoV-2 NSP6: in silico binding mechanistic analysis. *J Mol Med* **2020**;98:1659–73.
40. Fidock DA, Rosenthal PJ, Croft SL, et al. Antimalarial drug discovery: efficacy models for compound screening. *Nat Rev Drug Discov* **2004**;3:509–20.
41. Trager W, Jensen JB. Human malaria parasites in continuous culture. *Science* **1976**;193:673–5.
42. Mendoza-Martinez C, Galindo-Sevilla N, Correa-Basurto J, et al. Antileishmanial activity of quinazoline derivatives: synthesis, docking screens, molecular dynamic simulations and electrochemical studies. *Eur. J. Med. Chem* **2015**;92:314–31.
43. Temraz MG, Elzahhar PA, El-Din ABA, et al. Anti-leishmanial click modifiable thiosemicarbazones: design, synthesis, biological evaluation and in silico studies. *Eur J Med Chem* **2018**;151:585–600.
44. Bekhit AA, Hymete A, Damtew A, et al. Synthesis and biological screening of some pyridine derivatives as anti-malarial agents. *J Enzyme Inhib Med Chem* **2012**;27:69–77.
45. Bekhit AA, Fahmy HTY. Design and synthesis of some substituted 1H-Pyrazolyl-oxazolidines or 1H-Pyrazolyl-thiazolidines

- as anti-inflammatory-antimicrobial agents. *Archiv Der Pharmazie* **2003**;336:111–8.
46. Sanner MF. Python: a programming language for software integration and development. *J Mol Graph Model* **1999**;17: 57–61.
  47. Trott O, Olson AJ. AutoDock Vina: improving the speed and accuracy of docking with a new scoring function, efficient optimization, and multithreading. *J Comput Chem* **2010**;31: 455–61.
  48. Elghoneimy LK, Ismail MI, Boeckler FM, et al. Facilitating SARS CoV-2 RNA-dependent RNA polymerase (RdRp) drug discovery by the aid of HCV NS5B palm subdomain binders: in silico approaches and benchmarking. *Comp Biol Med* **2021**;134:104468.
  49. Bekhit AA, Nasralla SN, El-Agroudy EJ, et al. Investigation of the anti-inflammatory and analgesic activities of promising pyrazole derivative. *Eur J Pharm Sci* **2022**;168:106080.
  50. Abraham MJ, Murtola T, Schulz R, et al. GROMACS: high performance molecular simulations through multi-level parallelism from laptops to supercomputers. *SoftwareX* **2015**;1–2:19–25.
  51. Mark P, Nilsson L. Structure and dynamics of the TIP3P, SPC, and SPC/E water models at 298 K. *J Phys Chem A* **2001**;105: 9954–60.
  52. Bussi G, Donadio D, Parrinello M. Canonical sampling through velocity rescaling. *J Chem Phys* **2007**;126:014101.
  53. Berendsen HJC, Postma JPM, Gunsteren WFv, et al. Molecular dynamics with coupling to an external bath. *J Chem Phys* **1984**;81:3684–90.
  54. Parrinello M, Rahman A. Polymorphic transitions in single crystals: a new molecular dynamics method. *J Appl Phys* **1981**;52:7182–90.
  55. Darden T, York D, Pedersen L. Particle mesh Ewald: an N-log(N) method for Ewald sums in large systems. *J Chem Phys* **1993**;98:10089–92.
  56. Hess B, Bekker H, Berendsen HJC, Fraaije JGEM. LINCS: a linear constraint solver for molecular simulations. *J Comp Chem* **1997**;18:1463–72.
  57. Huang J, MacKerell AD Jr. CHARMM36 all-atom additive protein force field: validation based on comparison to NMR data. *J Comp Chem* **2013**;34:2135–45.
  58. Zoete V, Cuendet MA, Grosdidier A, Michielin O. SwissParam: a fast force field generation tool for small organic molecules. *J Comp Chem* **2011**;32:2359–68.
  59. McGibbon RT, Beauchamp KA, Harrigan MP, et al. MDTraj: a modern open library for the analysis of molecular dynamics trajectories. *Biophys J* **2015**;109:1528–32.
  60. Turner PX. Version 5.1. 19. Center for Coastal and Land-Margin Research, Oregon Graduate Institute of Science and Technology, Beaverton, OR; **2005**.